Bull. Mater. Sci., Vol. 33, No. 1, February 2010, pp. 21–26. © Indian Academy of Sciences.

Zn/ZnO core/shell nanoparticles synthesized by laser ablation in aqueous environment: Optical and structural characterizations

S C SINGH*, R K SWARNKAR and R GOPAL

Department of Physics, University of Allahabad, Allahabad 211 002, India

MS received 10 October 2008; revised 16 September 2009

Abstract. **Zn/ZnO core/shell nanoparticles are synthesized by pulsed laser ablation (PLA) of Zn metal plate in the aqueous environment of sodium dodacyl sulfate (SDS). Solution of nanoparticles is found stable in the colloidal form for a long time, and is characterized by UV-visible absorption, transmission electron microscopy (TEM), photoluminescence (PL) and Raman spectroscopic techniques. UV-visible absorption spectrum has four peaks at 231, 275, 356, and 520 nm, which provides primary information about the synthesis of core-shell and elongated nanoparticles. TEM micrographs reveal that synthesized nanoparticles are monodispersed with three different average sizes and size distributions. Colloidal solution of nanoparticles has significant absorption in the green region, therefore, it absorbs 514·7 nm light of Ar^+ laser and emits in the blue region centred at 350 and 375 nm, violet at 457 nm and green at 550 nm regions. Raman shift is observed at 300 cm^{-1} with PL spectrum, which corresponds to $^3E_{2N}$ and E_{3L} mode of vibrations of ZnO shell layer. Synthesis mechanism of Zn/ZnO core/shell nanoparticles is discussed.**

Keywords. **Pulsed laser ablation in aqueous media; II–VI semiconductor; core-shell nanoparticles; green photoluminescence; Raman scattering.**

1. Introduction

Due to their size and shape dependent properties, nanodimensional semiconductor materials have shown their great interest in optoelectronics, electronics, sensing, energy storing and harvesting applications. Binary semiconductor oxides such as ZnO, CdO, SnO_2 and In_2O_3 have innumerable applications and are now widely used as transparent conductive oxides (TCOs). Zinc oxide is mostly a *n*-type, II–VI, wide direct bandgap, semiconducting material. Being of its high optoelectronic efficiency relative to the indirect bandgap group IV crystals, it is considered as a reliable material for visible and near ultraviolet applications. Wurtzite zinc oxide has wide bandgap (3·37 eV), high exciton binding energy (≈ 60 meV) at room temperature, and high dielectric constant, therefore, possesses important applications in the fabrication of electronic and optical devices such as UV/blue lasers (Huang *et al* 2001; Johnson *et al* 2001) and LEDs. ZnO has noncentrosymmetric C^4_{6v} wurtzite crystal symmetry, hence it is found to be an interesting material for nonlinear second-harmonic generation and wave mixing in nanoscale cavities (Johnson *et al* 2002). It is transparent to most of the solar spectrum; therefore, widely used as window material in solar cells, optical waveguides, light modulators and optical sensors. Applications of ZnO are going on increasing in current decade in the fabrication of switching elements, transistors (Arnold *et al* 2002), lasers (Huang *et al* 2001; Johnson *et al* 2001) and detectors and therefore, controlled synthesis of good quality zinc oxide nanostructures such as nanocrystals (Singh and Gopal 2008a,b), nanowires (Xiang *et al* 2007; Guo *et al* 2008), nanobelts (Pan *et al* 2001; Kong *et al* 2004), nanotubes (Kong *et al* 2004) and other nanoarchitectures (Lao *et al* 2002; Kong and Wang 2003) is very important. Several routes are employed for the synthesis of ZnO nanomaterials including salvothermal (Dev *et al* 2006), thermal evaporation (Pan *et al* 2001; Kong *et al* 2004), solid-state pyrolysis (Wang *et al* 2003), sol–gel synthesis (Haase *et al* 1998), sputtering (Chen *et al* 1998), chemical vapour deposition (Gorla *et al* 1999; Xiang *et al* 2007), and molecular beam epitaxy (Agashe *et al* 2004) etc.

Metal core–metal oxide shell nanoparticles have several unique optical, photo catalytic and electronic properties neither shown by bare metal nor by metal oxide nanostructures. Physical and chemical properties of these materials are tunable and dependent on the thickness of the shell layer. Varying the ratio of core diameter and shell thickness, large shift in the optical emission and absorption is reported (Chen *et al* 2004).

Among all of the reported physical and chemical routes to produce nanomaterials, laser ablation is widely used for the synthesis of metallic and non-metallic nanostruc-

*Author for correspondence (Subhash_laserlab@yahoo.co.in)

tures in gas phase. Fojtik and Henglein (1993) and Cotton *et al* (1993, 1996) have used several liquids as ablation media to produce colloidal solution of nanoparticles, which are found to be simple and versatile tools for the synthesis of highly stable, monodispersed, chemical contamination free particles. Laser ablation in liquid media is also used for resizing and reshaping of nanoparticles produced by other conventional routes (Hodak *et al* 2000; Link *et al* 2000). Synthesis of noble metal nanoparticles by laser ablation in liquid media is extensively studied but there are a few reports on active transition metals and their oxide nanoparticles using this approach. Recently we have reported synthesis of Zn–ZnO (Singh and Gopal 2007) as well as ZnO/ZnOOH (Singh and Gopal 2008a, b) composite nanomaterials by laser ablation of zinc plate in aqueous solution of SDS using second harmonics of Nd : YAG laser.

Synthesis of Zn core/ZnO shell nanoparticles using PLA of Zn plate in 10 mM aqueous solution of SDS is the main theme of present communication. Synthesized particles are spherical as well as elongated in shape with Zn core and ZnO shell layer. Emission of shorter wavelengths (350 nm, 375 nm and 457 nm) light from the sample excited with higher wavelength laser light (514·7 nm) put some novelty in the present work and exhibits upconversion property of the sample. Enhanced green luminescence from synthesized nanoparticles excited by visible light is also an interesting and important finding of the work.

2. Experimental

Experimental arrangement for the synthesis of colloidal solution of nanomaterials using pulsed laser ablation in aqueous media is described elsewhere (Singh and Gopal 2007), and briefly high purity zinc target (99·99%, Johnston Mathey, UK), placed on the bottom of glass vessel containing 30 ml aqueous solution of 10 mM SDS, was allowed to irradiate with focused output of 1064 nm from pulsed Nd : YAG laser (Spectra Physics, Quanta Ray, USA) operating at 35 mJ/pulse energy, 10 ns pulse width and 10 Hz repetition rate for 2 h. As synthesized colloidal suspension was yellowish in colour and found stable for a long time. UV-visible absorption spectrum of as synthesized colloidal solution was recorded using Perkin Elmer, Lambda-35 double beam spectrophotometer after ultrasonification (35 kHz, 200 W, Apex instruments, Pvt. Ltd.). A drop of colloidal solution of nanoparticles was placed on the colloidan coated copper grid after ultrasonification (Advance Ultrasonic bath model As-150), and dried below the tungsten lamp. TEM images of nanoparticles were recorded using Philips, Morgagni-268 Transmission electron microscope operating at 70 kV. Photoluminescence and Raman spectra of as synthesized colloidal nanoparticles were recorded using 514·7 nm line of Ar^+ ion laser as excitation source and Acton 0·5 M triple grating monochromator with PMT detector for recording emitted/scattered light. Solution was placed in a quartz cell and excited by vertically downward light. Emitted/scattered light was collected on the slit of monochromator in the right angle geometry from the direction of excitation.

3. Results

UV-visible absorption spectrum of as synthesized colloidal solution of nanoparticles has four absorption maxima lying at 230, 278, 358 and 532 nm, as shown in figure 1. The UV peak at 230 nm is due to the transition of inner shell electron to the conduction, which is almost reported in the case of UV-visible absorption of all metal and metal oxide nanoparticles. As there are few reports on the surface plasmon absorption (SPR) of zinc metal nanoparticles, but recently, Lee and coworkers (Lee *et al* 2005) have reported SPR absorption at 255 nm for zinc nanocrystals embedded into SiO_2 matrix. We suggest that the peak at 278 nm is due to the surface plasmon absorption of zinc core nanoparticles, which is shifted towards red due to shell effect of ZnO. Absorption peak at 358 nm corresponds to SPR peak of ZnO shell layer, while that of the peak at 532 nm corresponds to the defect level or electron trap level in the Zn core/ZnO shell nanoparticles.

The bandgap of semiconductor materials will increase with the decrease in particle size, which leads to the shift of the absorption edge towards high energy side, which is the so called quantum size effect. The optical bandgap of as synthesized colloidal solution i.e. Zn core/ZnO shell is studied by UV-visible optical absorbance spectra. The optical bandgap, E_g, is determined from the absorbance

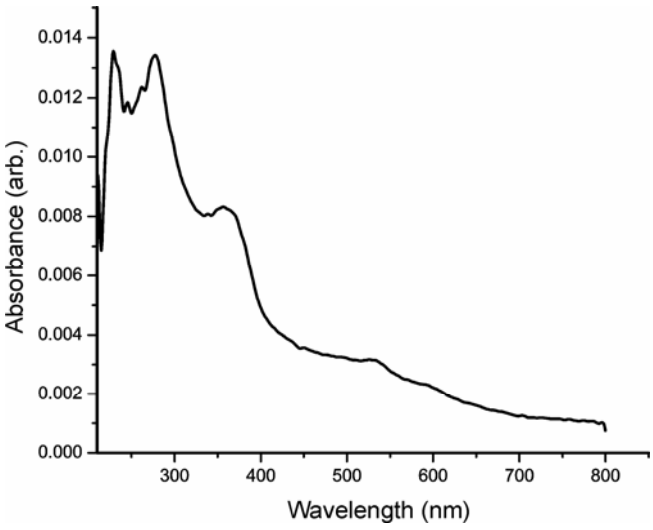

Figure 1. UV-visible absorption spectrum of colloidal solution of nanoparticles synthesized by laser ablation in the solution of 10 mM SDS at *RT* (20°C).

spectra, where a steep increase in the absorption is observed due to the band–band transition using the general relation

$$(\alpha h\nu)^n = B(E - E_g),$$

where B is a constant related to the effective masses of charge carriers associated with valence and conduction bands, E_g the bandgap energy, $E = h\nu$ the photon energy, and $n = 1/2$ or 2, depending on whether the transition is indirect or direct, respectively. The intersection of the slope of $(\alpha h\nu)^2$ vs $h\nu$ curve on the x-axis provides bandgap energy of the sample. Tauc plot of Zn core/ZnO shell nanoparticles is displayed in figure 2. Nature of the plot is in such a way that there are two intercepts for $\alpha = 0$ at 3·45 and 3·88 eV, which corresponds for bandgap of ZnO shell and combination of Zn core and ZnO shell layer. Full scale of the Tauc plot for UV-visible data is displayed in the inset.

Transmission electron microscopic images of Zn/ZnO nanoparticles are illustrated in figure 3 at the scale of (A) 1 μm and that of (B) 500 nm. There are some elongated large sized core/shell nanoparticles having 500 nm average length and 300 nm average width with almost 100 nm shell layer thickness as illustrated in figure 3(A). On the scale of 500 nm, there are large number of monodispersed spherical particles with almost 180 nm average diameter of Zn core, and 15 nm thick layer of ZnO shell. Large number of particles smaller than 40 nm in diameter is also present along with large sized particles (figure 3C). TEM images of the particles on the scale of 200 nm and 100 nm are displayed in figure 4. Smaller size of particles with 15 nm average diameter is present along with larger, 225 nm average, sized particles. TEM image of a single Zn core/ZnO shell nanoparticle, having 210 nm dia. consisting of 180 nm size of zinc core and 15 nm thick layer of ZnO shell, is shown in figure 4(B).

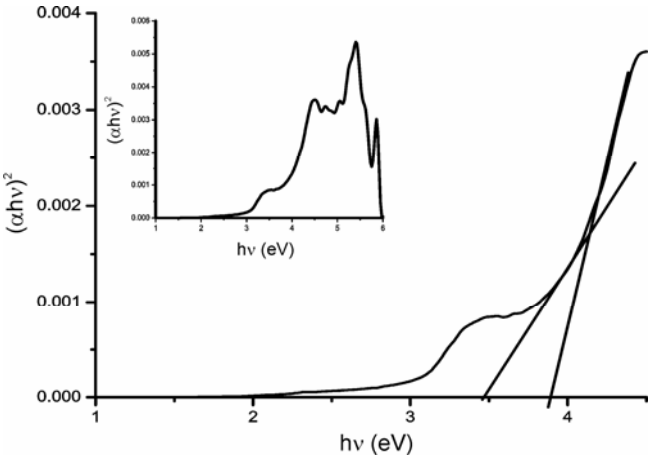

Figure 2. Tau plot of UV-visible absorption data for the calculation of bandgap energy at reduced scale. Tau plot of the UV-visible data at full scale is displayed inside the inset.

Photoluminescence spectra of Zn core/ZnO shell nanoparticles are recorded in the spectral regions of 320–485 nm and 515–620 nm. PL spectrum in the blue/violet region has three emission peaks centred at 250 nm, 375 nm and 457 nm (figure 5A). Out of the three emission peaks, one centred at 457 nm is the most intense. A broad emission peak centred at 550 nm is observed in the green (515–620 nm) region with spectral asymmetry towards longer wavelength side (figure 5B). Similar type of green emission and their applications in the cell imaging was reported from the ZnO core/polymer cell nanoparticles (Xiong *et al* 2008). There is one interesting thing that almost all semiconductor nanocrystals require UV light for their excitation, while sample reported in this literature is excited with 514·7 nm of Ar^+ ion laser and emit strong luminescence in higher as well as shorter wavelength side. Phenomenon of up conversion as well as down conversion is observed. The schematic diagram of the excitation/emission of/from the sample is illustrated in figure 5C. Electrons initially in the valence band may transit to the conduction band by two-photon absorption. Transition of some electrons from conduction band to valence band/anion vacancy level generates photons of 350 nm (3·53 eV)/375 nm (3·3 eV) wavelength corresponding to bandgap/anion vacancy level of the Zn/ZnO nanocrystals, while rest of the electrons transit to the defect level (cation at interstitial position) by losing some of their energy by collisional relaxation. Transition of electrons from interstitial cation level to the valence band/anion vacancy level emits blue/green photons of 457 nm (2·70 eV)/550 nm (2·25 eV) wavelengths. Some of the peaks, marked with *, in figure 5B, are assigned for the Raman scattering from the surface of Zn core/ZnO shell nanoparticles. Figure 6 illustrates Raman spectrum of the Zn core/ZnO shell nanoparticles. Raman shift peak at 109 cm^{-1} corresponds for the E_2 symmetry of wurtzite ZnO crystals, while that of the peak at 300 cm^{-1} is assigned for $^3E_{2N}$, E_{3L} mode of vibration of zinc oxide.

4. Discussion

4.1 *Mechanism for synthesis of Zn, ZnO and Zn core/ZnO shell nanoparticles*

Laser ablation in active liquid media is of particular interest due to its high non-equilibrium processing, which allows synthesis of novel phases of nanostructured materials. The most important difference between laser ablation of solid in vacuum or diluted gas and in liquid environment is the strong confinement of species in the laser produced plasma by liquid. Therefore, a series of mechanism including generation, transformation and condensation of plasma plume produced laser ablation of solid in liquid environment takes place in the condition of the liquid confinement. The confinement of plume by

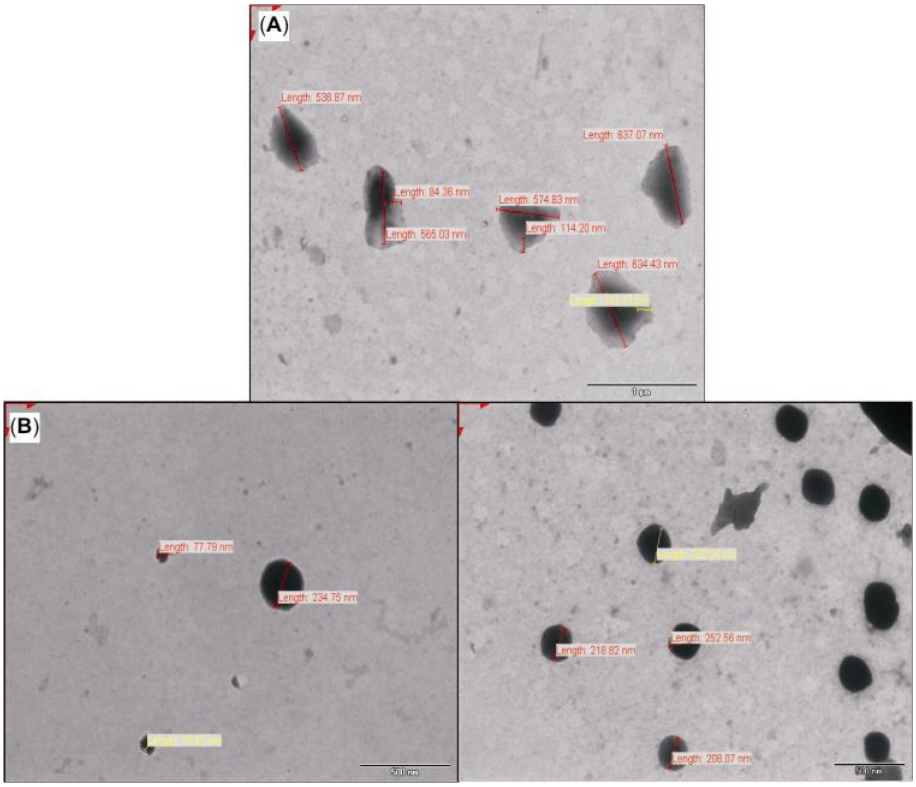

Figure 3. TEM micrographs of Zn/ZnO nanoparticles on the scale of (**A**) 1 μm and (**B**) 500 nm synthesized by pulsed laser ablation.

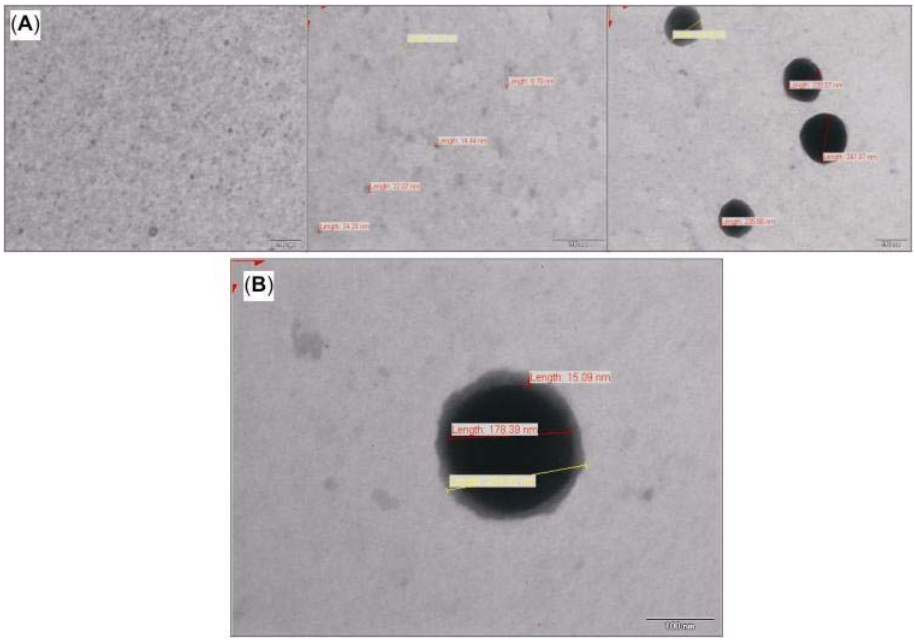

Figure 4. TEM micrographs of Zn/ZnO nanoparticles on the scale of (**A**) 200 nm and (**B**) 100 nm synthesized by pulsed laser ablation.

liquid can greatly influence the thermodynamic and kinetic properties of the evolution of the plasma plume, and creates a different environment of the condensing phase formation from that of laser ablation of solids in vacuum or diluted gas. Yang has discussed thermodynamic, kinetic and liquid confinement effect aspects of the plasma

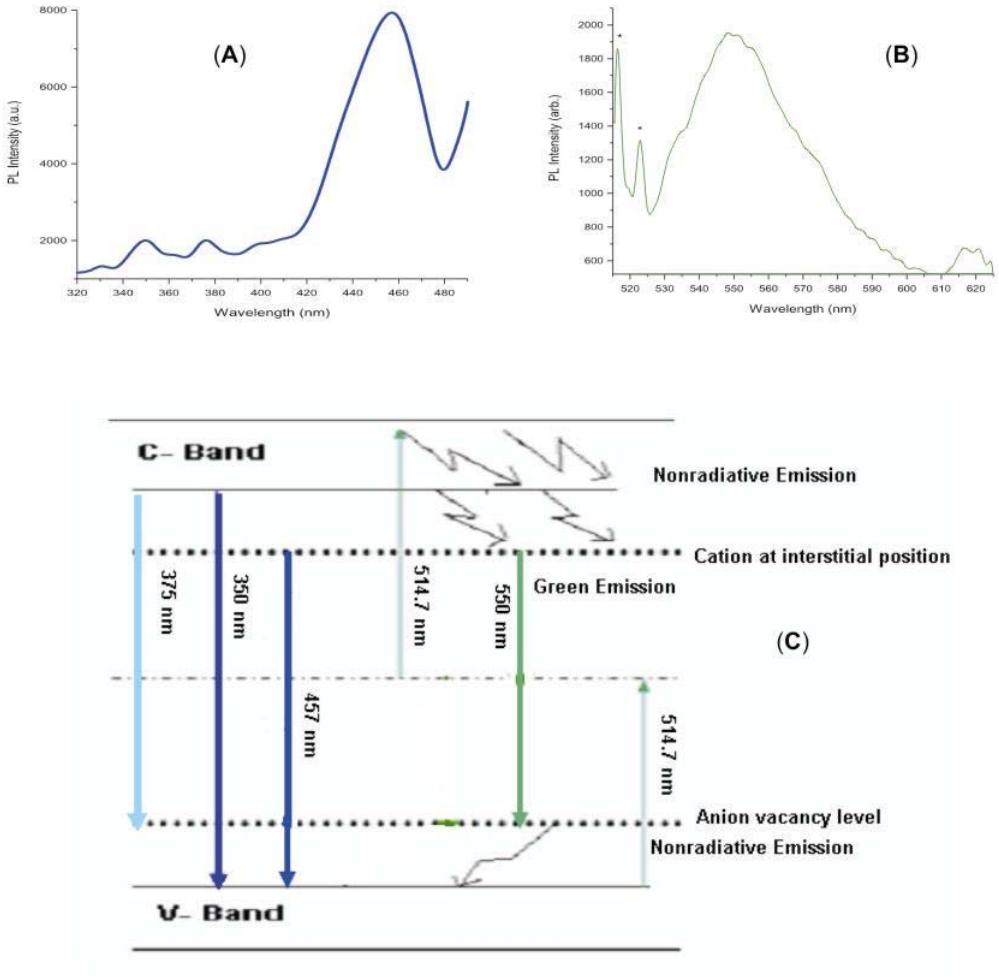

Figure 5. Photoluminescence spectrum as synthesized colloidal solution of Zn/ZnO core-shell nanoparticles in the (**A**) blue/violet region, (**B**) green region excited with 514·5 nm of Ar^+ laser (*represents Raman scattering) and (**C**) proposed schematic view of the absorption and emission of light.

plume produced by laser solid interaction in liquid environment (Yang 2007). When front part of the laser pulse interacts with the solid target, it induces plasma plume on the surface of the target, which gets supersonically expanded after absorbing rest part of the laser pulse and feels pressure induced by shock wave. There may be various chemical reactions and physical processes among the ablated metal species, solvent molecules, and surfactant molecules, which induces the formation of several molecular species in the solution, which can act as seeds for the growth of nanoparticles. Plasma plume gets cool and hence condense in the form of nanoparticles after losing its energy by expanding against pressure induced by shock wave. Plume also gets condensed on the surface of target and is applicable for surface coating of the material. The structure, morphology, size and hence properties of nanoparticles will depend on the temperature, pressure and composition of plasma plume, which itself is dependent on laser ablation parameters and nature of liquid media.

On the basis of above reaction mechanisms, formation of Zn, Zn–ZnO nanocomposite and Zn core/ZnO shell structures took place in the following three steps: (i) generation of high temperature and high pressure plasma after the interaction of laser light with matter, (b) ultrasonic and adiabatic expansion of the plasma plume against the liquid environment, cooling of the plasma and formation of cold clusters and (iii) with the extinguishment of the plasma, the produced clusters encounter the solvent and surfactant molecules in the solution, which induces some chemical reactions and capping effects. There is a competitive mechanism between aqueous oxidation of zinc clusters to form $Zn(OH)_2$ molecules, which can easily dissociate to form ZnO molecules, and SDS capping for termination of growth.

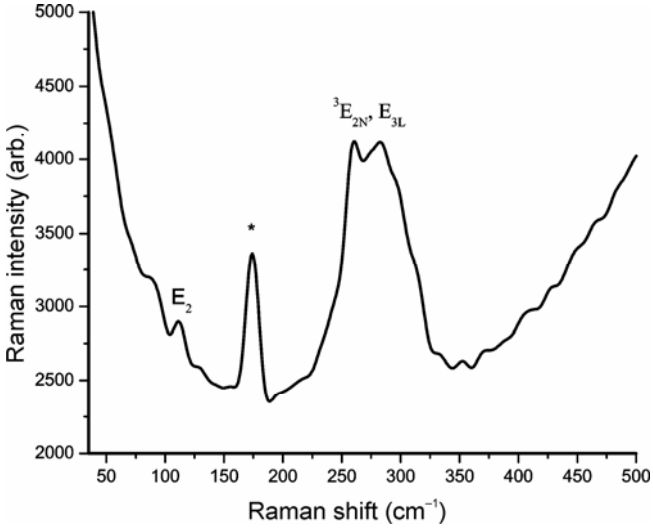

Figure 6. Raman scattering spectrum of as synthesized colloidal solution of Zn/ZnO nanoparticles (*Raman scattering from the quartz tube).

$$Zn\ (cluster) + 2H_2O = Zn\ (OH)_2 + H_2,$$

$$Zn\ (OH)_2 = ZnO + H_2O.$$

If the surfactant concentration is small (<CMC), the aqueous oxidation effect will be dominant. At lower laser irradiance and smaller amount of surfactant, small number of atoms is vapourized, which gets aqueous oxidized and form ZnO clusters of 1–20 nm diameter. In the case of large laser irradiance or/and higher surfactant concentration large number of atoms get vapourized, which form larger metal clusters of 100 nm diameters and get capped by SDS molecules to prevent oxidation. When surfactant concentration is low (near CMC), surfaces of the nanoparticles with large diameter are weakly capped by SDS, which gets oxidized to form Zn core of large diameter with small thickness of ZnO shell. As time passes it may be possible to increase thickness of the shell layer. It means that mostly large sized particles synthesized by laser ablation in near CMC of surfactant have Zn core and ZnO shell, while those of small sized ones are completely of zinc oxide as in the case of present investigation. At higher surfactant concentration strong capping on the surface of the nanoparticles is achieved, which prevents it for aqueous oxidation and synthesis of pure zinc nanoparticles is done.

Acknowledgements

Authors are thankful to the Defence Research Development Organization (DRDO), New Delhi, for financial support during the work. They are grateful to the Director, AIIMS, New Delhi, for providing TEM facility. CSIR, New Delhi, is also acknowledged by one of the authors (SCS) for providing him with a Senior Research Fellowship (SRF).

References

Agashe C, Kluth O, Hupkes J, Zastrow U, Rech B and Wuttig M 2004 *J. Appl. Phys.* **95** 1911

Arnold M, Avouris Ph, Pan Z W and Wang Z L 2002 *J. Phys. Chem.* **B107** 659

Chen Y, Bangall D M, Koh H, Park K, Hiraga K, Zhu Z and Yao T 1998 *J. Appl. Phys.* **84** 3912

Chen X, Lou Y and Burda C 2004 *Int. J. Nanotech.* **1** 105

Cotton T M, Neddersen J and Chumanov G 1993 *Appl. Spectrosc.* **47** 1959

Cotton T M, Sibbald M S and Chumanov G 1996 *J. Phys. Chem.* **100** 4672

Dev A, Kar S, Chakrabarti S and Chaudhuri S 2006 *Nanotechnol.* **17** 1533

Fojtik A and Henglein A 1993 *Ber. Bunsen-Ges. Phys. Chem.* **97** 252

Gorla C R, Emanetoglu N W, Liang S, Mayo W E, Lu Y, Wraback M and Shen H 1999 *J. Appl. Phys.* **85** 2595

Guo R, Nishimura J, Matsumoto M, Higashihata M, Nakamura D and Okada T 2008 *Jap. J. Appl. Phys.* **47** 741

Haase M, Weller H and Henglein A 1998 *J. Phys. Chem.* **92** 482

Hodak J H, Henglein A, Giersig M and Hartland G V 2000 *J. Phys. Chem.* **B104** 11708

Huang M H, Mao S, Feick H, Yan H, Yiying W, Kind H, Weber E, Russo R and Yang P 2001 *Science* **292** 1897

Johnson J C, Yan H, Schaller R D, Haber L H, Saykally R J and Yang P 2001 *J. Phys. Chem.* **B105** 113875

Johnson J C, Yan H, Schaller R D, Petersen P B, Yang P and Saykally R J 2002 *Nano Lett.* **2** 279

Kong X Y and Wang Z L 2003 *Nano Lett.* **3** 1625

Kong X Y, Ding Y and Wang Z L 2004 *J. Phys. Chem.* **B108** 570

Lao J Y, Wen J G and Ren Z F 2002 *Nano Lett.* **2** 1287

Link S, Burda C, Nikoobakht B and El-Sayed M A 2000 *J. Phys. Chem.* **B104** 6152

Pan Z W, Dai Z R and Wang Z L 2001 *Science* **291** 1947

Singh S C and Gopal R 2007 *Bull. Mater. Sci.* **30** 291

Singh S C and Gopal R 2008a *Phys.* **E40** 724

Singh S C and Gopal R 2008b *Phys. Chem.* **C112** 2812

Xiang B, Wang P, Zhang X, Dayeh S A, Aplin D P R, Soci C, Yu D and Wang D 2007 *Nano Lett.* **7** 323

Xiong H, Xu Y, Ren Q and Xia Y 2008 *J. Am. Chem. Soc.* **130** 3522

Wang Z, Zhang H, Zhang L, Yuan J, Yan S and Wang C 2003 *Nanotechnol.* **11** 14

Yang G W 2007 *Prog. Mater. Sci.* **52** 648